

# Integrated decision-making model for groundwater potential evaluation in mining areas using the cusp catastrophe model and principal component analysis

Xiaofei Sun <sup>a,c</sup>, Yingzhi Zhou <sup>b,d,\*</sup>, Linguo Yuan <sup>a,\*\*</sup>, Xianfeng Li <sup>d</sup>, Huaiyong Shao <sup>b</sup>, Xixi Lu <sup>c</sup>

<sup>a</sup> Faculty of Geosciences and Environmental Engineering, Southwest Jiaotong University, Chengdu, 611756, China

<sup>b</sup> College of Earth Science, Chengdu University of Technology, Chengdu, 610059, China

<sup>c</sup> Department of Geography, National University of Singapore, Kent Ridge, 117570, Singapore

<sup>d</sup> Natural Resources and Planning Bureau of Nanchong, Nanchong, 637000, China



## ARTICLE INFO

### Keywords:

Groundwater potential mapping  
Groundwater management  
Spatial modeling  
Multicriteria decision-making  
Evaluation indicators

## ABSTRACT

**Study Region:** Panxi mining area (15061 km<sup>2</sup>, located in Sichuan, China).

**Study Focus:** This study aims to delineate groundwater potential zones in mining areas using a new method based on the cusp catastrophe model (CCM) and principal component analysis (PCA). First, 13 indicators were selected from natural and anthropogenic dimensions, and a comprehensive analysis of the indicators was performed using PCA. Second, the results of the PCA were considered as control variables, and the CCM was used for groundwater potential evaluation modeling. Finally, the receiver operating characteristic (ROC) curve was used to validate the new method and compare it with catastrophe fuzzy membership functions (CFMFs).

**New Hydrological Insights for the Region:** The results suggest that the area under the ROC curve of the success and prediction rate accounted for approximately 0.85 and 0.76, respectively, in the new method, which were higher than those in the CFMFs. The largest area (39 %) with groundwater potential in the study area has a “moderate” groundwater potential status, followed by an area (28 %) with a “good” status, an area (20 %) with a “poor” status, and areas (12 % and 1%) with “very good” and “very poor” statuses, respectively. The groundwater potential in the study area was unevenly distributed and changed drastically. Topography, drainage density, and land use/land cover had the highest contribution in the modeling process.

## 1. Introduction

Groundwater is one of the most extensive freshwater resources worldwide and is closely related to daily life and material infrastructure for human survival and development (Aeschbach-Hertig et al., 2012; Jha, 2013). Because of its constant temperature, extensive and continuous cycle regeneration, good water quality, and stability, it has become an essential and reliable source of water supply for countries and regions with different climatic zones and economic development levels (Todd and Mays, 2005). With the rapid

\* Natural Resources and Planning Bureau of Nanchong, Nanchong, 637000, China.

\*\* Corresponding author at: Faculty of Geosciences and Environmental Engineering, Southwest Jiaotong University, Chengdu, 611756, China.

E-mail addresses: [zhouyz793@163.com](mailto:zhouyz793@163.com) (Y. Zhou), [lgyuan@swjtu.edu.cn](mailto:lgyuan@swjtu.edu.cn) (L. Yuan).

development of the social economy, China's demand for mineral resources has increased (Wen et al., 2019), and long-term and large-scale mining has caused severe damage to the environment. In particular, drainage pits cause the groundwater level to decrease, which consequently affects the groundwater flow system (Zhu et al., 2014). This condition, in turn, poses severe threats to the lives of residents and the safety of irrigation water (Post et al., 2020). Therefore, the construction of a suitable model is urgently needed for the evaluation of groundwater potential in mining areas for the protection and sustainable management of groundwater resources in such areas.

In traditional groundwater exploration methods, the various factors that control the occurrence and movement of groundwater are not always considered, the associated cost is extremely high, and the timeliness is poor (Oh et al., 2011; Razandi et al., 2015). In recent years, remote sensing (RS) and geographic information system (GIS) technologies have provided systematic, rapid, and excellent configurations for processing large and complex spatial data, affording opportunities for understanding the complex issues related to groundwater exploration (Murmu et al., 2019). Numerous studies have also been performed to evaluate groundwater potential using machine learning models based on GIS and RS technologies. For example, Kumar and Krishna (2018) used geospatial techniques and an analytic hierarchy process (AHP), which have strong applicability in determining indicator weights, to delineate groundwater potential areas in the Indian Rhargarh and Hazaribagh regions. However, the results obtained are highly subjective and vary according to the opinions of experts (Dai et al., 2009). Manap et al. (2014) applied the frequency ratio model (FRM) to create a groundwater level map of Malaysia's Langat Basin and verified the evaluation results with an accuracy of 84.78 %. Although the calculation and output processes of the FRM are straightforward and easy to understand, the evaluation results are directly related to the number of samples used in the evaluation (Yilmaz, 2009). Ozdemir (2011) used the logistic regression method (LRM) in the GIS environment and selected 17 factors to construct the groundwater spring potential map of the Sudan Mountain in Central Turkey. The LRM offers the advantages of simplicity, fast training speed, and reasonable probability interpretation of the output variables. However, it can only be applied in the case of large sample sizes, which often leads to the multicollinearity problem (Asar, 2017). Naghibi et al. (2017a) stated that the random forest (RF) and genetic algorithm optimized random forest methods are more effective than the support vector machine (SVM) for groundwater potential evaluation. Although the RF has high accuracy and efficiency and can directly process high-dimensional data, it is complex and requires more training time than other similar algorithms (Cheng et al., 2014). Lee et al. (2019) applied an artificial neural network (ANN) to predict the groundwater level in Yangpyeong County of South Korea and suggested that the river water level is the main factor affecting groundwater level fluctuations. ANNs can automatically adjust the weight of an evaluation indicator and feature strong adaptability; however, they often suffer from the overfitting problem when the training samples are insufficient or over-trained (Krizhevsky et al., 2012). Some scholars have also used various combination of models to evaluate the groundwater potential. Examples include the fuzzy AHP (Azimi et al., 2018), weighted index overlays and two-dimensional electrical resistivity tomography (Gyeltshen et al., 2020), evidence belief function and boosted regression tree (Kordestani et al., 2019), evidential belief function and tree-based models (Naghibi et al., 2019), ANN and real AdaBoost (Nguyen et al., 2020), and gray clustering method and AHP (Sahoo et al., 2017). Although the abovementioned methods can quantitatively or qualitatively reflect the groundwater potential, they tend to seek for a "superior" model through an inter-comparison of multiple models, without adequate attention to maximizing the learning from these models (Karimi et al., 2020). In addition, most of the existing multiobjective decision-making methods are uncertain in terms of solving the nonlinear and discontinuity problems between evaluation indicators, and their calculation process is complicated (Singh et al., 2009).

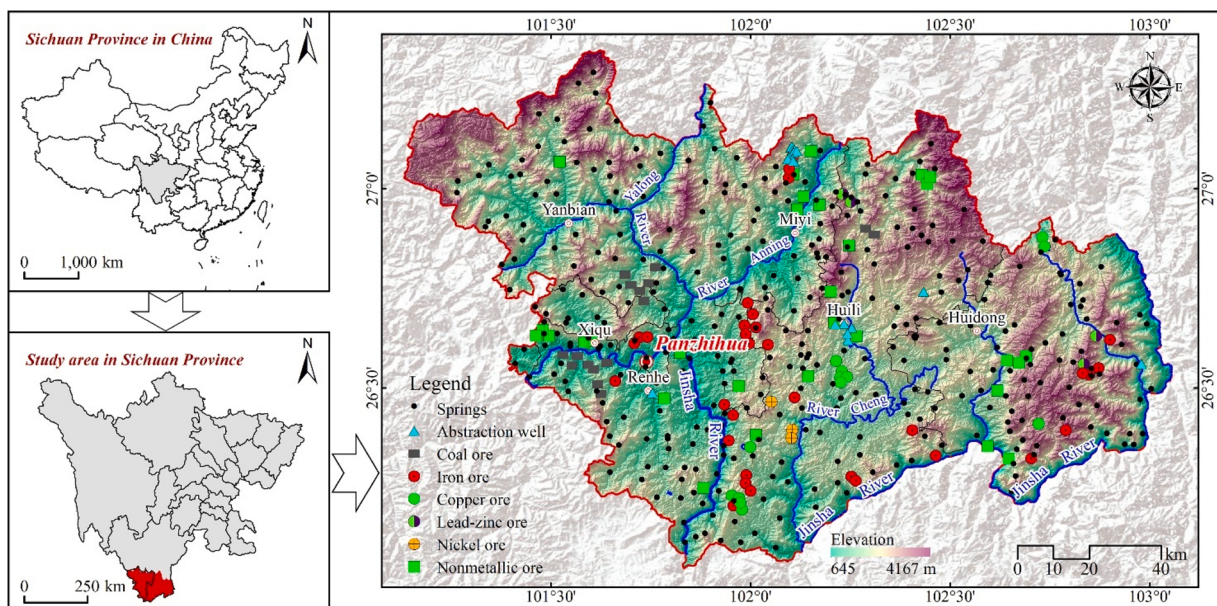


**Fig. 1.** Location of the study area.

Catastrophe theory (CT) is a system theory proposed by Rene Thom. This theory is based on topology, the singularity theory, and the system structural stability theory; it is used to study the mutations caused by gradual changes (Zeeman, 1979). Compared with other methods, CT shows acceptable performance and is an objective approach to solve the catastrophic problem of discontinuous changes in natural systems and social fields (Liu et al., 2015). It has also been widely used in studies on groundwater potential (Ahmed et al., 2015; Al-Abadi et al., 2015; Sadeghfam et al., 2016). In addition, Sadeghfam et al. (2020a,b, 2021) applied CT to groundwater over-abstraction, groundwater vulnerability, and groundwater pollution and achieved good results. These aforementioned studies prove that an integrated model based on CT can effectively improve the objectivity of research results. Such an approach typically involves the use of catastrophe fuzzy membership functions (CFMFs). However, uncertainties in the CFMFs arise when determining the priority sequence of control variables in catastrophe subordinate systems. To solve the uncertainties in existing studies using CT to evaluate groundwater potential, the coordinate transformation technology was employed for applying the cusp catastrophe model (CCM) in CT and principal component analysis (PCA) in groundwater potential evaluation modeling. Thus, the specific objectives of this study are as follows: 1) to consider the Panxi mining area (China) as an example, collect spatiotemporal data related to groundwater potential in the study area, and establish an evaluation indicator system; 2) to use PCA for natural and anthropogenic indicators and perform a statistical analysis of the PCA results; and 3) to develop a method suitable for the groundwater potential evaluation in mining areas based on the PCA results and CCM and verify the effectiveness of this method.

## 2. Study area

The Panxi mining area is located in the transition zone between the Tibetan Plateau and Yunnan–Guizhou Plateau (Fig. 1). Southwestern warm and wet monsoons, originating from the Indian Ocean, are obstructed by the Hengduan mountains, resulting in the Foehn effect in the study area (Huan-cheng and McConchie, 2001). The wet and dry seasons in the study area are clearly distinguishable. The annual average temperature is 16 °C–17 °C, the precipitation is 800–1200 mm, and the annual evaporation in the valley area is three to six times the precipitation (Wang et al., 2018). The study area is characterized by alpine valleys as dominant landforms at an altitude of 645–4167 m. This area constitutes China's substantial ferrous and non-ferrous metal mining base (Wu and Zhang, 2019). Mining in the study area has led to a decline in the groundwater level, which has increased the competition between

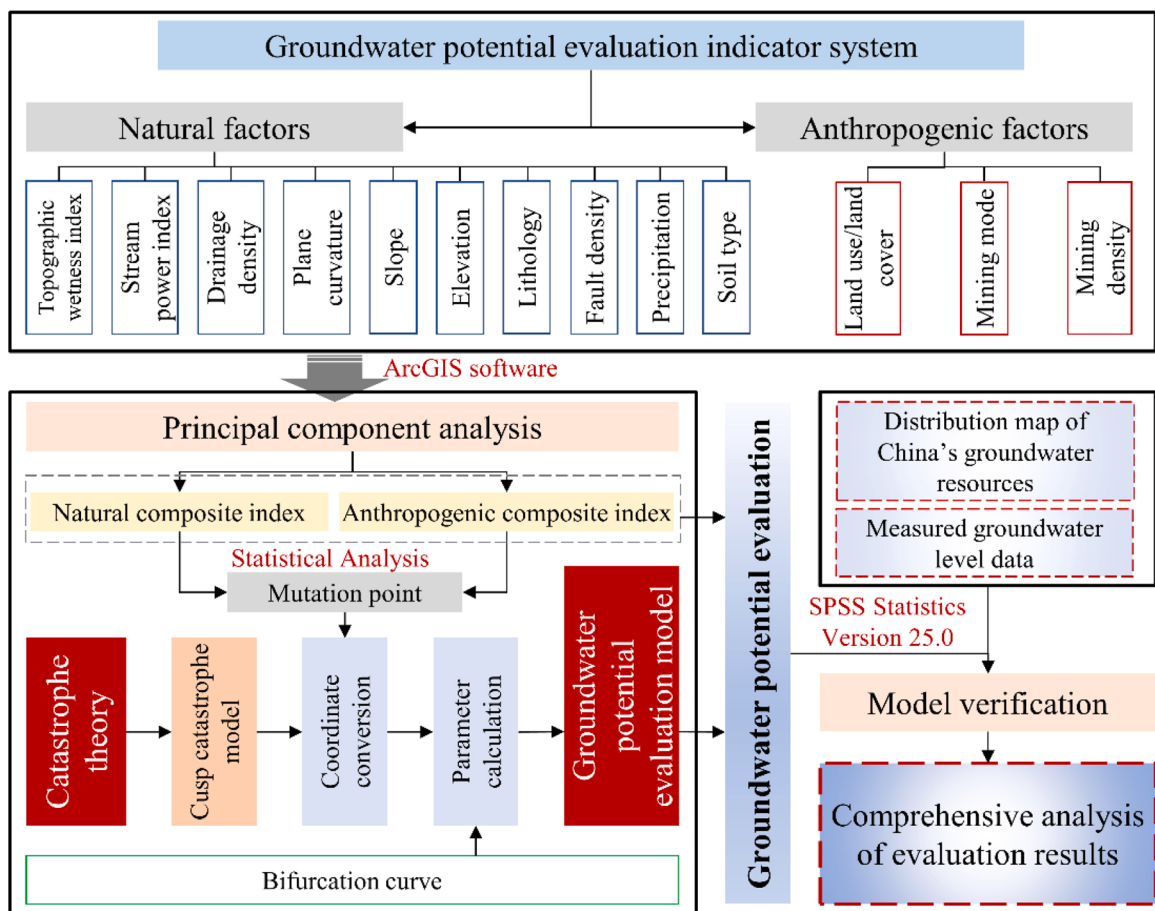


Fig. 2. Flowchart of the groundwater potential evaluation method.

residents' living and irrigation water, especially during winter when the rainfall declines, resulting in a decrease in the groundwater level. Therefore, it is necessary to accurately evaluate the groundwater potential of the study area and understand its change process, given the significance of the groundwater potential in the management and protection of groundwater resources in a particular area.

According to the characteristics of the aquifer group and the occurrence conditions of groundwater, the study area can be divided into four types of aquifers (Dai, 2016):

- 1) Quaternary loose rock weak aquifer: It is mainly composed of gravel, sand, and sandy clay. It features loose lithology, large porosity, and low water content.
- 2) Clastic rock weak water-bearing group: This group is distributed over most regions in the study area and is dominated by sandstone, siltstone, and mudstone. Hence, it is a relatively water-resistant layer. The rock formation has developed fissures and exposed many springs, and the spring flow rate is 0.1–1.2 L/s.
- 3) Basalt water-bearing rock group: It is composed of basalt, purple tuffaceous sandstone, and tuff. Surface weathering cracks have been developed, with a weathering thickness of 0.5–1.2 m. The overall water content is low, and the spring flow is less than 0.1 L/s.
- 4) Carbonate water-bearing rock group: It is composed of dolomite, shale, and limestone. Its water content is high, and the spring flow rate is 8.7 L/s.

### 3. Methodology

The proposed method involves three steps (Fig. 2). 1) An indicator system based on natural and anthropogenic factors was constructed, and the PCA was used for a comprehensive analysis of these factors. 2) The PCA results were considered as control variables, coordinate transformation technology was used for applying the CCM to the groundwater potential evaluation modeling, and the feasibility of the model was verified. 3) The new integrated method was applied for the groundwater potential evaluation of the study area in 2000, 2010, and 2020, and characteristics of the groundwater potential distribution and change process within the study area were analyzed.

#### 3.1. Evaluation indicator system and data collection

##### 3.1.1. Evaluation indicator system

The factors that influence groundwater potential are geology, topography, meteorology, hydrology, vegetation, and human activities (Jenifer and Jha, 2017). Accordingly, based on previous studies (Chen et al., 2018; Rizeei et al., 2019), an evaluation indicator

**Table 1**

Evaluation indicators and reasons for their selection.

Factor	Indicator	Reasons for selection
Natural factors	Topographic wetness index (TWI)	TWI has a positive relationship with the recharge of groundwater aquifers (Naghibi et al., 2017b). It can quantitatively simulate dry and wet soil moisture conditions and is the most commonly used indicator for static soil moisture content.
	Stream power index (SPI)	One of the most important factors in controlling slope erosion processes is SPI. Regions with high stream power have high erosion potentiality (Gómez-Gutiérrez et al., 2015). SPI can better describe the characteristics of water convergence and divergence.
	Drainage density	The study area is affected by the Foehn effect, resulting in high temperatures and significant evaporation in low-altitude areas, whereas peaks and ridges feature low temperatures, less evaporation, and relatively higher precipitation. The surface water on top of the mountain is drained to the low-altitude areas, which can well supplement the groundwater at low-altitude areas.
	Plane curvature	The plane curvature of the ground is important, as concave surfaces are more suitable for holding surface water, thus helping in recharging the area.
	Slope	Slope affects the accumulation of runoff and the filtration rate of rainwater, which is crucial for predicting the groundwater potential; the higher the slope angle, the lower is the infiltration and recharge.
	Elevation	Surface runoff mainly flows from high to low altitudes. Therefore, low-altitude areas ensure high surface moisture levels and enrich groundwater aquifers through long ponding times. A flat or mild slope also helps detain the water flow (Serele et al., 2020), thus reducing flow velocity.
	Lithology	Aquifers are controlled by lithology. Thus, lithology is essential in the evaluation of groundwater potential. Primary and secondary openings in rocks affect the occurrence and distribution of groundwater (Arulbalaji et al., 2019).
	Fault density	A high fault density can be used to speculate secondary porosity, as most fault systems serve as conduits for the movement and storage of groundwater (Krishnamurthy et al., 2000).
Anthropogenic factors	Precipitation	Precipitation is an essential source of groundwater recharge and plays a vital role in the groundwater potential evaluation.
	Soil type	Soil permeability is directly related to the effective porosity and is strongly influenced by the grain shape, size of grains, adsorbed water, and void ratio (Punnia and Jain, 2005).
	Land use/land cover (LULC)	LULC reflects the interaction between human activities and natural systems and demonstrates the intensity of human activities that affect available groundwater resources (Lerner and Harris, 2009).
	Mining mode	Different mining modes cause different degrees of damage to groundwater.
	Mining density	Mining density is the number of mines mined per unit area; the higher the mining density, the more severe is the damage to the underground aquifer.

system for the study area was constructed, considering both natural and anthropogenic aspects. In this indicator system, 10 natural factors and three anthropogenic factors were included; the reasons governing the selection of these indicators are listed in [Table 1](#).

### 3.1.2. Data collection and processing

The data types and sources adopted in this study, with regard to the evaluation indicator system, are listed in [Table 2](#). The collected data were processed according to an evaluation indicator system; this processing method is detailed below:

- 1) The digital elevation model (DEM) for the study area was obtained from the Geospatial Data Cloud (China). Using the spatial analysis tools in ArcGIS, most of the natural factors were derived from DEM data, including the TWI, SPI, slope, elevation, and water system.

$$TWI = \ln\left(\frac{E}{tanF}\right) \quad (1)$$

$$SPI = E \times tanF \quad (2)$$

where  $E$  is the specific catchment area, and  $F$  is the local slope gradient.

- 2) LULC-type information was obtained through a classification of Landsat images. The SVM-based supervised classification method was applied to the study area images using ENVI 5.3, and 120 points were randomly selected for assessing the classification precision. The validation accuracy for this classification was 85 %.
- 3) The mining scope was extracted from high-spatial-resolution images (Google and Gaofen-1 images) and Landsat images. The information extraction method employed involved a visual interpretation. An accuracy of 93 % was realized, which was validated by randomly selecting 60 points.
- 4) The mining modes were obtained through the mining concession of the study area and converted into raster data using ArcGIS.
- 5) The density analysis tool in ArcGIS was used to convert the drainage, faults, mines, and residential areas into raster data. The lithology and soil type are spatial data and only require projection conversion and rasterization.
- 6) According to the data from eight monitoring stations located in and around the study area, the precipitation data were interpolated in ArcGIS in order to convert statistical data into spatial data. The interpolation method employed was Kriging, which is widely used for meteorological data ([Bargaoui and Chebbi, 2009](#)).
- 7) The Gauss–Kruger projection was used in this study; the dimensions of the evaluation unit were 250 m × 250 m.

### 3.1.3. Standardization of indicators

To ensure that the influences of different indicators on the groundwater potential were comparable, the indicator values were standardized to the range of -1 to 1 ([Fig. 3](#)). As the TWI, SPI, drainage density, plane curvature, slope, elevation, fault density, precipitation, and mining density are continuous spatial data, they can be standardized directly. However, the lithology, LULC, soil types, and mining modes are categorical spatial data, which must be quantified prior to the standardization. The quantitative methods for the lithology, LULC, soil type, and mining mode are listed in [Table 3](#).

## 3.2. Modeling process

### 3.2.1. PCA

The principal component function in ArcGIS was used to conduct the PCA transformation of the natural and anthropogenic factors. Based on the calculation results, the first  $n$  principal components (cumulative contribution rate exceeding 90 %) and their contribution rates were selected for the weighted calculation ([Poon et al., 2011](#)), and the natural composite index ( $N$ ) and anthropogenic composite

**Table 2**

Types and sources for data collection.

Datatype	Data sources	Format
Landsat images	Orbit numbers include 131041 (2000/01/02, 2010/03/18, 2020/03/13), 130042 (2000/01/02, 2010/03/18, 2020/03/29), and 129042 (2000/02/12, 2010/02/07, 2020/02/19). Among these, the images in 2000 and 2010 are Landsat-5 TM, and the images in 2020 are Landsat-8 OLI. The spatial resolution is 30 m. Source: <a href="http://www.gscloud.cn/">http://www.gscloud.cn/</a>	Raster
High-resolution images	Google Earth (2009/03/30–2010/11/18), Gaofen-1 image (2020/02/20, 2020/04/05, 2020/03/28). The spatial resolution is 2 m.	Raster
DEM data	The spatial resolution is 90 m. Source: <a href="http://www.gscloud.cn/">http://www.gscloud.cn/</a>	Raster
Precipitation	This study collected data from eight monitoring stations in the study area and in surrounding areas (2000.1–2000.12; 2010.1–2010.12; 2019.1–2020.12). Source: <a href="http://data.cma.cn/">http://data.cma.cn/</a>	Text
Lithology, fault	Geological maps (scales of 1: 200,000). Source: <a href="http://www.ngac.cn/">http://www.ngac.cn/</a>	Vector
Soil type	The spatial resolution is 250 m. Source: Soil Information Service Platform ( <a href="http://www.soilinfo.cn/map/">http://www.soilinfo.cn/map/</a> )	Raster
Mining concession	In 2020, the study area had 149 underground mining, 34 unitized mining, and 306 open-pit mining areas. Source: Sichuan Geological Survey Institute	Vector
Inventory of springs	There are 374 springs in the study area. Source: <a href="http://www.ngac.cn/">http://www.ngac.cn/</a>	Vector

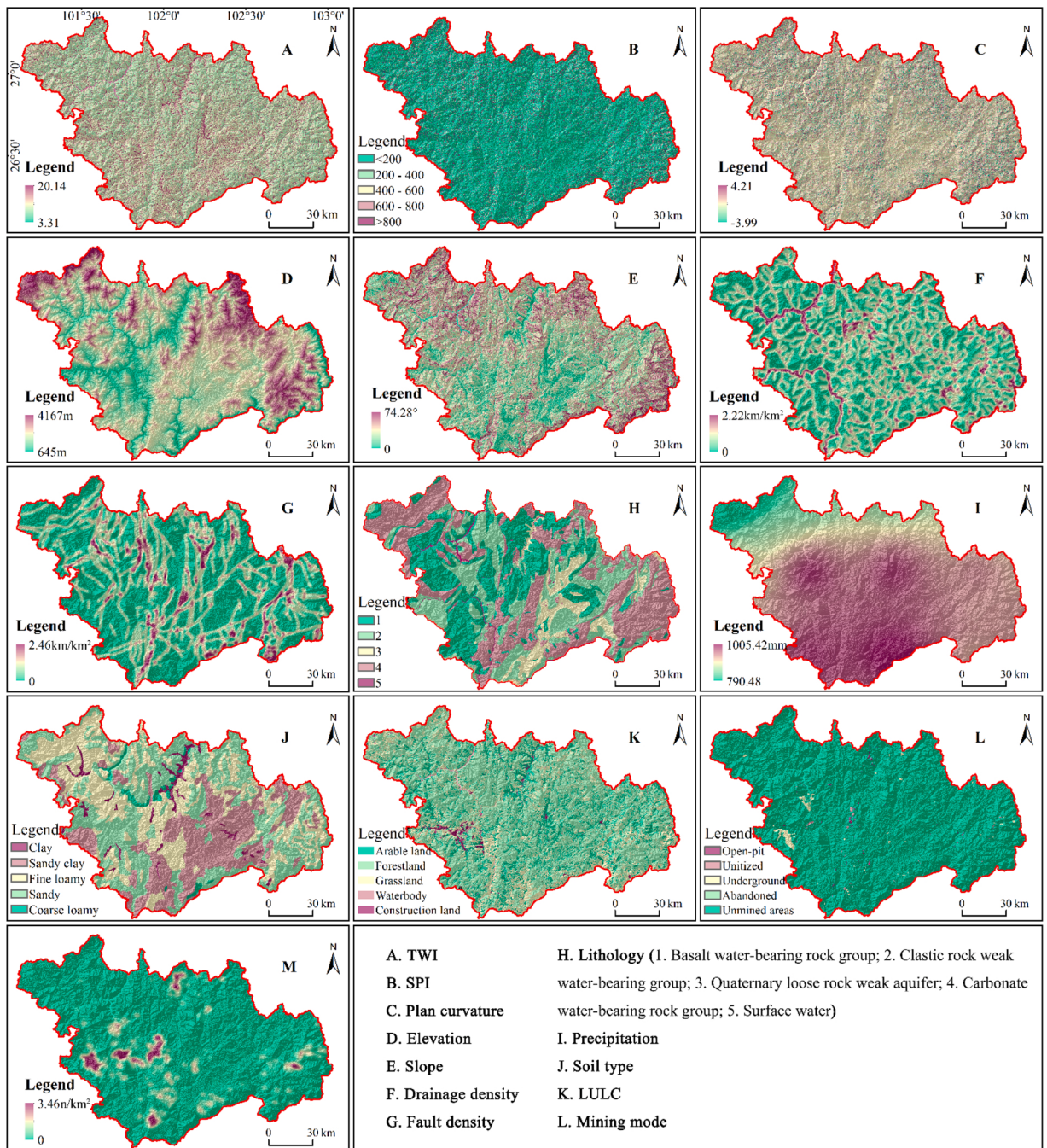


Fig. 3. Evaluation indicators for the study area in 2020.

index ( $S$ ) of the study area in 2000, 2010, and 2020 were obtained. For complete details regarding the comprehensive PCA, please refer to the work of [Shao et al. \(2014\)](#).

### 3.2.2. CCM

In CT, when two control variables exist, the catastrophe model is a cusp-type model. Therefore, the natural and anthropogenic composite indices were considered as the control variables, and the CCM was used to construct the groundwater potential evaluation model.

#### (1) Equilibrium surface

**Table 3**

Quantification of qualitative indicators.

Indicator	Quantitative method or reference	Category	Rating
Lithology	Yeh et al., 2009; Thapa et al., 2017	Surface water	5
		Carbonate water-bearing rock group	4
		Quaternary loose rock weak aquifer	3
		Clastic rock weak water-bearing group	2
		Basalt water-bearing rock group	1
		Waterbody	5
LULC	Agarwal et al., 2013, 2016	Forestland	4
		Grassland	3
		Arable land	2
		Construction land	1
		Coarse loamy	5
		Sandy	4
Soil type	Kumar et al., 2014	Fine loamy	3
		Sandy clay	2
		Clay	1
		Unmined areas	5
		Abandoned mining	4
		Underground mining	3
Mining mode	The mining modes in the study area mainly include open-pit mining, underground mining, unitized mining, and abandoned mines	Unitized mining	2
		Open-pit mining	1

The equilibrium surface determined using the three-dimensional coordinates  $(m_1, n_1, n_2)$  of the CCM is expressed in Eq. 3. To accurately simulate the mapping relationship among the control variables—natural composite index ( $N$ ), anthropogenic composite index ( $S$ ), and state variable of the groundwater potential ( $GP$ )—all the coefficients in Eq. 3 were considered as non-zero constants.

$$n_2 = am_1^3 + bn_1m_1 \quad (3)$$

In Eq. 3,  $m_1 = m_0$  is set, that is,  $m_1$  is set to a fixed value;  $n_1$  and  $n_2$  form a linear relationship. Thus, the equilibrium surface is composed of straight lines parallel to the plane  $n_1$  on  $n_2$  (Fig. 4).

As shown in Fig. 4, when  $n_1 > 0$ ,  $m_1$  slowly increases with an increase in  $n_2$ . When  $n_1 < 0$ ,  $m_1$  continues to increase with  $n_2$ . However, when  $m_1$  reaches a specific range, a small increase in  $n_2$  can lead to a sharp and discontinuous increase in  $m_1$ . Thus, establishing the conversion relationship between  $(m_1, n_1, n_2)$  and  $(GP, N, S)$  is a key aspect of applying the CCM to evaluate groundwater potential.

## (2) Coordinate conversion

The original coordinate system  $(m_1, n_1, n_2)$  is converted into a new coordinate system  $(GP, N, S)$  when the translation is set to  $(m_{11}, n_{11}, n_{22})$ , and the rotation angle around the  $m_1$ -axis is  $\beta$ . The conversion equation is as follows:

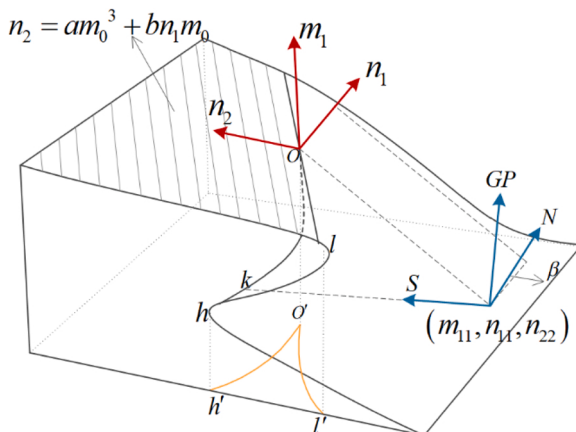


**Fig. 4.** Schematic of the equilibrium surface and coordinate transformation of the CCM.  $o'l'$  and  $o'h'$  are bifurcation curves, which are the projected singularities set on the control variable plane of the two extreme curves  $(oh, ol)$  passing through the origin of the original coordinates (Shao et al., 2021).

$$\begin{cases} m_1 = GP + m_{11} \\ n_1 = N\cos\beta + S\sin\beta + n_{11} \\ n_2 = -N\sin\beta + S\cos\beta + n_{22} \end{cases} \quad (4)$$

In Fig. 4, the coordinate origin ( $m_{11}, n_{11}, n_{22}$ ) of the new coordinates ( $GP, N, S$ ) also lies on the original coordinate system. Therefore,  $n_2 = am_{11}^3 + bn_1m_{11}$  is set as the  $N$ -axis of the natural composite index. Thus, the straight line is the intersection of the plane passing through the origin of the new coordinate system and the equilibrium surface. The new coordinate system is derived by translating the original coordinate system and rotation  $\beta$  around the  $GP$ -axis. Accordingly,

$$\sin\beta = \frac{bm_{11}}{\sqrt{1+b^2m_{11}^2}}, \cos\beta = \frac{1}{\sqrt{1+b^2m_{11}^2}} \quad (5)$$

### (3) New coordinates

Based on the PCA results, the mutation points  $N_1, S_1, N_2$ , and  $S_2$  were obtained through a statistical analysis of the natural composite index ( $N$ ) and the anthropogenic composite index ( $S$ ) (Fig. 5).

A plane perpendicular to the  $N$ -axis through point  $(GP_1, N_1, S_1)$  is created in the new coordinate system  $(GP, N, S)$ . As  $(GP_1, N_1, S_1)$  is the mutation point in the groundwater potential and the origin of the original coordinate system is also a mutation point, the created plane passes through the origin of the original coordinate system. Thus, point  $(GP_1, N_1, S_1)$  in the original coordinate system is  $(GP_1 + m_{11}, N_1\cos\beta + S_1\sin\beta + n_{11}, -N_1\sin\beta + S_1\cos\beta + n_{22})$ , and the direction vector of the  $m_1$ -axis is  $(0, \cos\beta, \sin\beta)$ . The equation of this plane can be expressed as follows:

$$n_1\cos\beta - n_2\sin\beta = 0 \quad (6)$$

Substituting the insertion point  $(GP_1 + m_{11}, N_1\cos\beta + S_1\sin\beta + n_{11}, -N_1\sin\beta + S_1\cos\beta + n_{22})$  into Eq. 6 and combining the solutions of Eq. 5 yield

$$\frac{n_{11}}{\sqrt{1+b^2m_{11}^2}} - \frac{bn_{22}m_{11}}{\sqrt{1+b^2m_{11}^2}} + N_1 = 0 \quad (7)$$

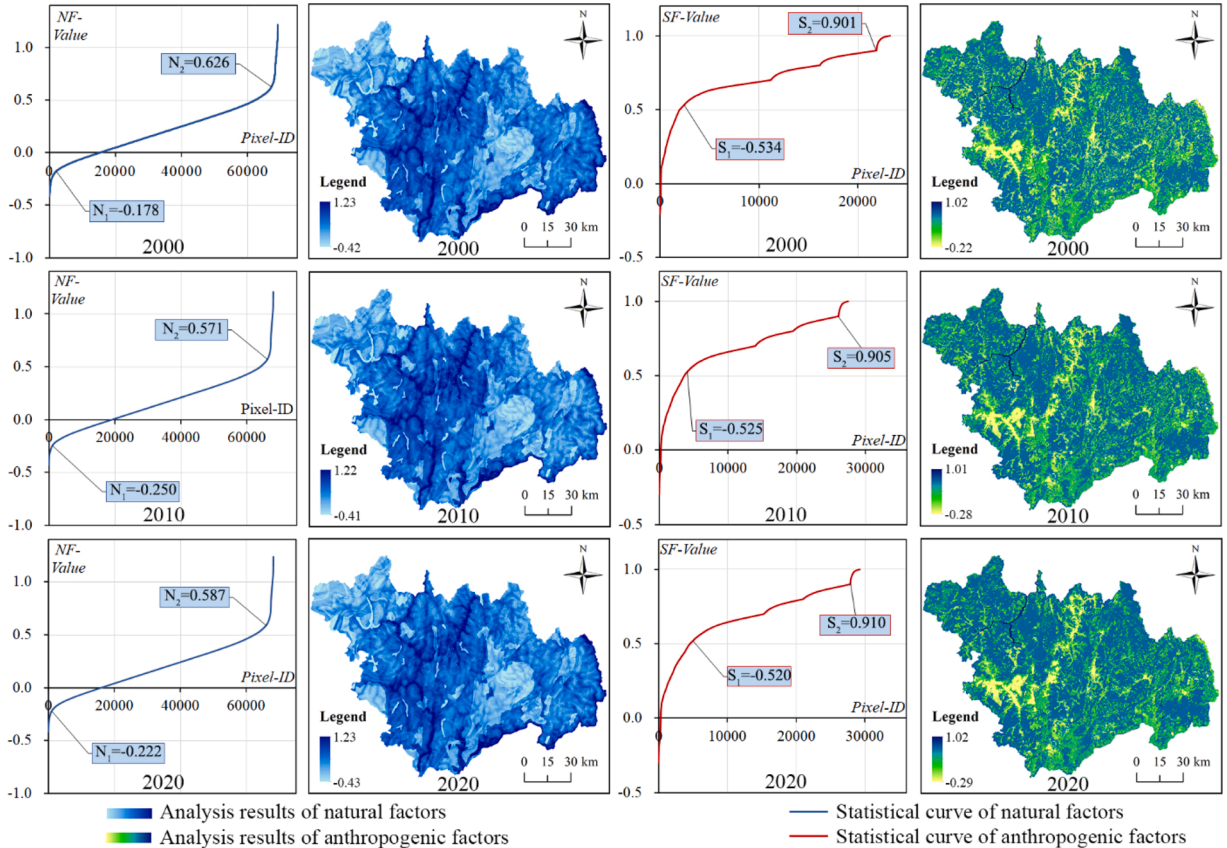


Fig. 5. Mutation points of the natural and anthropogenic composite indices (2000, 2010, and 2020).

Similarly, when the new coordinates  $(GP, N, S)$  undergo mutation again at point  $(GP_2, N_2, S_2)$ , the coordinate point  $k$  ( $GP_2 + m_{11}, N_2 \cos\beta + S_2 \sin\beta + n_{11}, -N_2 \sin\beta + S_2 \cos\beta + n_{22}$ ) serves as the intersection point (mutation point) of the  $N$ -axis and singularity set of the equilibrium surface. There are three roots of  $m_1$  at  $k$  point, i.e.,  $m_{11}$ ,  $m_{12}$ , and  $m_{13}$ . Thus,  $-N_2 \sin\beta + S_2 \cos\beta + n_{22} = am_1^3 + bm_1(N_2 \cos\beta + S_2 \sin\beta + n_{11})$  has three roots that satisfy the equation  $(m_1 - m_{11})(m_1 - m_{12})(m_1 - m_{13}) = 0$ . The three roots of this equation have two equal roots ( $m_{11} = m_{13}$ ). Thus, the following equation is obtained:

$$m_1^3 - (2m_{11} + m_{12})m_1^2 + (m_{11}^2 + 2m_{11}m_{12})m_1 - m_{11}^2m_{12} = 0 \quad (8)$$

Let Eq. 8 be equal to the coefficients of the equation  $-N_2 \sin\beta + S_2 \cos\beta + n_{22} = am_1^3 + bm_1(N_2 \cos\beta + S_2 \sin\beta + n_{11})$ . Combining the solutions of Eq. 5 yields

$$\begin{cases} 0 = 2m_{11} + m_{12} \\ \frac{b}{a} \left( \frac{N_2}{\sqrt{1+b^2m_{11}^2}} + \frac{S_2bm_{11}}{\sqrt{1+b^2m_{11}^2}} + n_{11} \right) = m_{11}^2 + 2m_{11}m_{12} \\ \frac{S_2}{\sqrt{1+b^2m_{11}^2}} - \frac{bN_2m_{11}}{\sqrt{1+b^2m_{11}^2}} + n_{22} = am_{11}^2m_{12} \end{cases} \quad (9)$$

In Fig. 4, point  $k$  is the mutation point of the groundwater potential. Thus, the groundwater potential undergoes transition from  $m_{11}$  to  $m_{12}$  at point  $k$ . Referring to previous results (Zhu, 2014), the transition amount can be represented as follows:

$$m_{11} = 1 + m_{12} \quad (10)$$

#### (4) Construction of evaluation model

On substituting Eqs. 4 and 5 into Eq. 3, the equilibrium surface  $(GP, N, S)$  after a coordinate transformation can be obtained, which can be expressed as follows:

$$(GP + m_{11})^3 + \frac{b}{a} \left( \frac{N}{\sqrt{1+b^2m_{11}^2}} + \frac{Sbm_{11}}{\sqrt{1+b^2m_{11}^2}} + n_{11} \right) (GP + m_{11}) + \frac{1}{a} \left( \frac{bNm_{11}}{\sqrt{1+b^2m_{11}^2}} - \frac{S}{\sqrt{1+b^2m_{11}^2}} - n_{22} \right) = 0 \quad (11)$$

Setting  $GP + m_{11}$  as unknown, the Cardano formula is employed to obtain the discriminant of Eq. 11, as follows:

$$W = 9 \left[ \frac{1}{a} \left( \frac{bNm_{11}}{\sqrt{1+b^2m_{11}^2}} - \frac{S}{\sqrt{1+b^2m_{11}^2}} - n_{22} \right) \right]^2 + 4 \left[ \frac{b}{a} \left( \frac{N}{\sqrt{1+b^2m_{11}^2}} + \frac{Sbm_{11}}{\sqrt{1+b^2m_{11}^2}} + n_{11} \right) \right]^3 \quad (12)$$

Eq. 12 represents a model for groundwater potential evaluation. To further strengthen the understanding of the groundwater potential distribution and the changing rules in the study area, the following criteria were designed. The CCM is a cubic equation (Eq. 3); hence, it consists of three unreal roots. When  $W < 0$ , Eq. 12 yields three unequal real roots, which implies that the groundwater potential corresponds to the “very poor” status. When  $W \geq 0$ , the natural breaks classification method (Liu et al., 2018) is applied to classify the results into statuses of “poor,” “moderate,” “good,” and “very good.”

#### (5) Model solution

Using Eqs. 7, 9, and 10, the values of the unknowns  $a, b, m_{11}, m_{12}, n_{11}$ , and  $n_{22}$  can be obtained. The solution steps are as follows:

- 1) Setting  $b$  as an arbitrary non-zero constant and assigning a value.
- 2) According to the six unknown coefficients, the bifurcation curve can be obtained ( $o'l', o'h'$ ) (Fig. 4). The bifurcation curve equation is as follows:

$$a \left( \sqrt{\frac{-bn_1}{3a}} \right)^3 + bn_1 \left( \sqrt{\frac{-bn_1}{3a}} \right) = n_2 \quad (13)$$

$$a \left( -\sqrt{\frac{-bn_1}{3a}} \right)^3 - bn_1 \left( \sqrt{\frac{-bn_1}{3a}} \right) = n_2 \quad (14)$$

- 3) The number of springs is a critical factor when modeling groundwater potential (Moghaddam et al., 2020). Therefore, 262 springs (70 % of the total number of springs) were selected as the sample dataset for the evaluation. Given a random  $b$  value, more than 90 % of the sample data were located away from the bifurcation curve, indicating that the value,  $b$ , meets the necessary requirements. Otherwise, the value for  $b$  needs to be reassigned (Fig. 6).

With the aforementioned steps and MATLAB, the trial algorithm was adopted to determine the values of  $a, b, m_{11}, m_{12}, n_{11}$ , and  $n_{22}$

(Table 4).

### 3.3. Model verification

Model verification is one of the most important steps in modeling. Without verification, the constructed evaluation model will have no scientific significance. The receiver operating characteristic (ROC) curve is a scientific approach for describing the efficiency of probabilistic and deterministic detection and forecasting systems; it is widely used in various fields, such as for groundwater potential evaluation (Pradhan, 2013). The area under the ROC curve (AUC) is also useful for quantifying the uncertainty in model predictions, while accounting for detection biases associated with the estimation (Zipkin et al., 2012).

In this study, 262 springs (70 % of the total number of springs) were selected as the sample dataset and 112 springs (30 % of the total number of springs) were selected as the validation dataset in order to assess the proposed model. The sample dataset was used to calculate the success rate of the evaluation results, and the verification dataset was used to calculate the prediction rate. Based on the evaluation indicator, the CFMFs were used to evaluate the groundwater potential, and a comparative analysis with the new integrated method was performed. In addition, the average groundwater level data from 18 wells were selected as a reference to further verify the accuracy of the evaluation results.

## 4. Results

### 4.1. Evaluation results

According to Eq. 12 and the coefficients presented in Table 4,  $N$  and  $S$  for the years 2000, 2010, and 2020 were employed to obtain the evaluation results for the study area (Fig. 7).

As shown in Table 5, the areas under the “moderate” and “good” statuses were the largest, followed by those under the “poor” and “very good” statuses; the areas under the “very good” status were the smallest. The evaluation results for 2020 were considered as an example, where the area under the “very good” status is  $1801.08 \text{ km}^2$ , accounting for 11.96 % of the total area, and that under the “good” status is  $4230.35 \text{ km}^2$ , accounting for 28.09 %. The abovementioned status is mainly distributed in the valley, which is located in the middle of the study area. The area under the “moderate” status is  $5821.46 \text{ km}^2$ , accounting for 38.65 %, and this area is distributed primarily toward the east and northwest regions of the study area. The area under the “poor” status is  $3021.13 \text{ km}^2$ , accounting for 20.06 %. Furthermore, the area under the “very poor” status is  $186.75 \text{ km}^2$ , accounting for 1.24 %; this area is mainly distributed in the mining and urban areas (e.g., Taiping – East district – Hongge area, Baima and Lixi – Lvshui). Overall, the groundwater potential evaluation results are consistent with those presented in a previous study (Jiang, 2005).

With regard to the changes in the groundwater potential that occurred from 2000–2020, the areas under the “very poor,” “poor,” and “good” statuses continue to increase, those under the “very good” status continue to decrease, and those under the “moderate” status initially increase and then decrease.

### 4.2. Verification results

Through a verification, the AUC values for the success rates of the evaluation results for 2000, 2010, and 2020 were obtained; these values were 0.847, 0.851, and 0.860, respectively (Fig. 8a). For the prediction rate curve, the results exhibited a trend similar to that of the success rate curve, and the AUC values were 0.755, 0.762, and 0.773 for 2000, 2010, and 2020, respectively (Fig. 8b). The success rate and the prediction rate of the new integrated method were higher than those of the CFMFs. Compared with the AUC classification performed by Yesilnacar and Topal (2005), the new integrated method exhibited reasonably good accuracy in terms of the spatial prediction of groundwater potential.

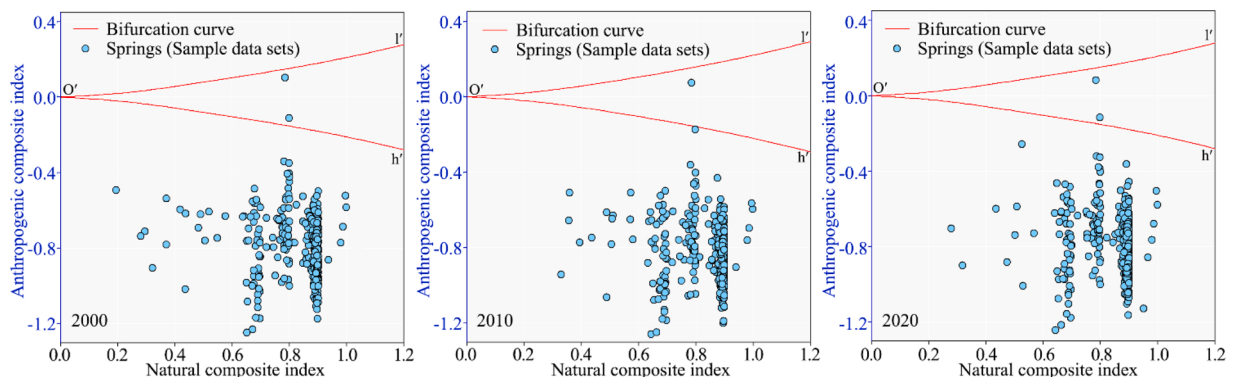


**Fig. 6.** Bifurcation curves  $o'l'$  and  $o'h'$ . More than 90 % of the sample data are located away from the bifurcation curve on the control plane in this figure. Hence, the relevant parameters in the evaluation model are deemed reasonable.

**Table 4**

Parameter values of the developed model.

Parameter	$a$	$b$	$m_{11}$	$m_{12}$	$n_{11}$	$n_{22}$
2000	-2.61	0.96	0.33	-0.67	-0.47	0.04
2010	-2.56	0.93	0.33	-0.67	-0.51	0.11
2020	-2.56	0.94	0.33	-0.67	-0.5	0.07

Legend:

- Study area (black outline)
- Very Poor (red square)
- Poor (orange-red square)
- Moderate (light blue square)
- Good (medium blue square)
- Very Good (dark blue square)

CCM-PCA: New integrated method      CFMF: Catastrophe fuzzy membership function

**Fig. 7.** Evaluation results for groundwater potential in the study area.

Moreover, the groundwater data observed in the field were in good agreement with the evaluation results (for 2020), with a correlation coefficient of 0.87, which is also higher than that for the CFMFs (Fig. 8c). The abovementioned verification results, therefore, demonstrate that the evaluation model developed in this study using the CCM and PCA achieves good performance in

**Table 5**

Area statistics for the groundwater potential status in the study area.

Method	Type	2000		2010		2020	
		Area (km <sup>2</sup> )	Percentage	Area (km <sup>2</sup> )	Percentage	Area (km <sup>2</sup> )	Percentage
New integrated method	Very Poor	78.63	0.52%	151.36	1.01%	186.75	1.24 %
	Poor	2840.69	18.86%	2862.76	19.01%	3021.13	20.06 %
	Moderate	5951.38	39.52%	6004.63	39.87%	5821.46	38.65 %
	Good	4178.63	27.75%	4192.26	27.84%	4230.35	28.09 %
	Very Good	2011.44	13.36%	1849.75	12.28 %	1801.08	11.96 %
CFMFs	Very Poor	53.38	0.35%	132.61	0.88%	156.75	1.04%
	Poor	2104.75	13.98%	2155.31	14.31%	2299.87	15.27%
	Moderate	5657.88	37.57%	5917.19	39.29%	5513.31	36.61%
	Good	6020.25	39.97%	5852.44	38.86%	6107.01	40.55%
	Very Good	1224.5	8.13%	1003.2	6.66%	983.81	6.53%

evaluating the groundwater potential.

## 5. Analysis and discussion

### 5.1. Analysis of groundwater potential changes

#### 5.1.1. “Very poor” status

The mineral resource development areas and the urban construction areas fall under the “very poor” status. Typical mines in these areas include the Zhiubaobao-Lanjian iron mine, Lala copper mine, Baima iron mine, Huashan coal mine, and Hongge iron mine. The “very poor” status of the groundwater potential in these areas can be attributed to two possible reasons. 1) Long-term and large-scale mining leads to increased land occupation in these areas. During mining, the pit drainage causes the groundwater level to decrease (Zhu et al., 2020). 2) Urban construction also leads to the conversion of arable land, forestland, grassland, wetland, and other types of coverage into residential, transportation, commercial, and industrial lands, thus increasing the impervious surface area and reducing the groundwater supply (Tsegaye et al., 2006; Okadera et al., 2019). From the perspective of the change process, the area under the “very poor” status increased from 2000 to 2020. In addition, the area under the “very poor” status showed an increase of 72.74 km<sup>2</sup> from 2000–2010, which represents an increase rate of 92.51 % (Fig. 9a, b). This is likely because the continuous increase in the intensity and scale of the development of mineral resources led to increased extraction of groundwater and mine drainage around the mining areas, resulting in a decline in the groundwater level (Zheng, 2012; Pigato and Tang, 2015). From 2010–2020, the area under the “very poor” status showed an increase of 35.39 km<sup>2</sup>, representing an increase rate of 23.38 %. Accordingly, the rapid expansion of urban construction is considered as the main reason for the increase in the area under the “very poor” status during this period (Fig. 9c).

Compared with the contribution of mining toward the increase in the area under the “very poor” status for the period from 2000–2010, the contribution toward the increase in the area under the “very poor” status from 2010 to 2020 is lower. This is likely because, in 2009, the Chinese government increased the supervision and management of mine geo-environment management projects, which helped restore the groundwater level in the mining areas to a certain extent (Grigg, 2017).

#### 5.1.2. “Poor” status

The area under the “poor” status is mainly distributed around the area under the “very poor” status; hence, it has good spatial

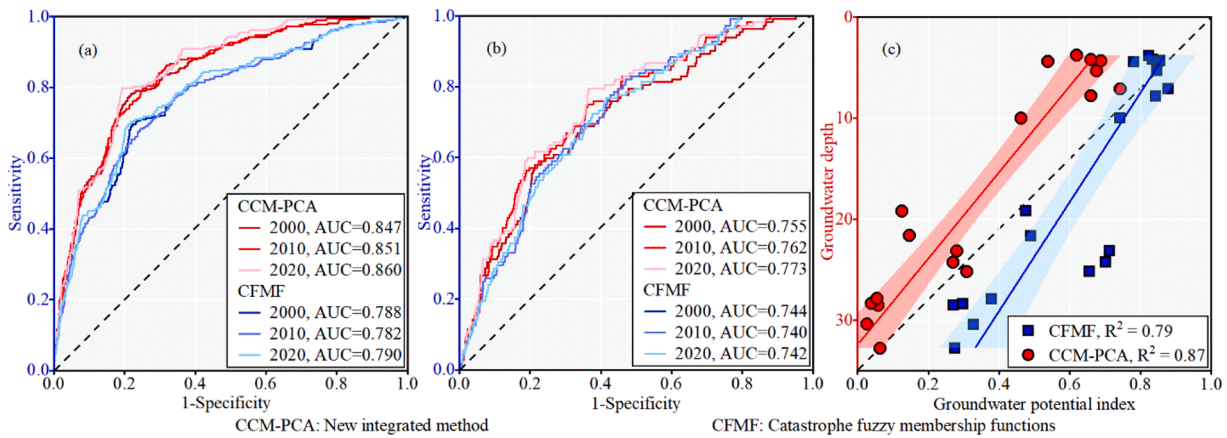
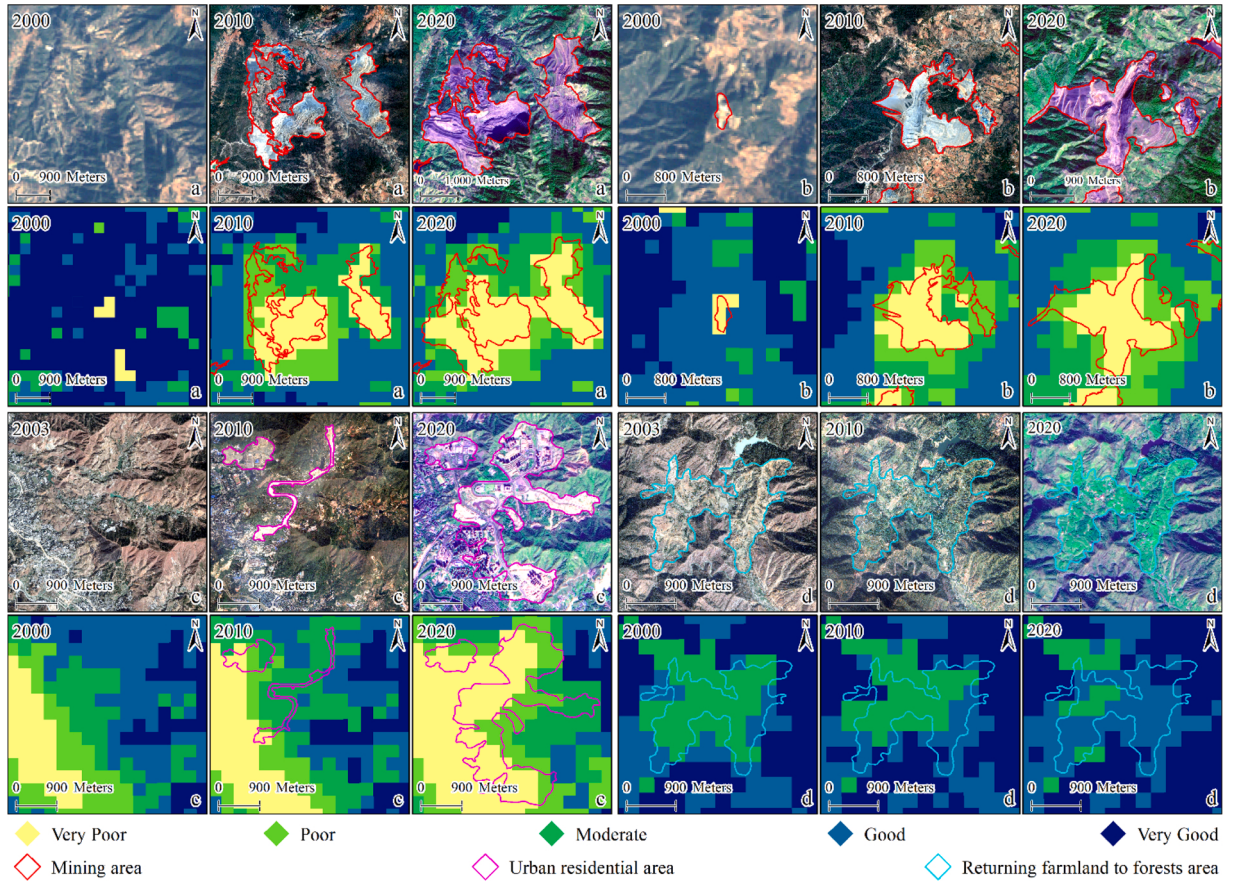


Fig. 8. Verification of evaluation results: (a) success rate; (b) prediction rate; and (c) comparison of evaluation results with on-site observation data.



**Fig. 9.** Evaluation results of groundwater potential in typical areas within the study area: (a–b) mining area; (c) urban residential area; and (d) conversion of farmlands to forest areas.

correlation with the distribution of the area under the “very poor” status. From 2000–2020, the area under the “poor” status showed an increase of  $180.44 \text{ km}^2$ , representing an increase rate of 6.35 %. The surrounding environmental pressure caused by mining and urban construction is considered as the main factor that causes the groundwater potential in this area to become “poor.” Furthermore, the area under the “poor” status is primarily located in the hillside, where the degree of evaporation exceeds that of precipitation, resulting in a further decrease in the groundwater potential (Zhong, 2000).

#### 5.1.3. “Moderate” status

The areas under the “moderate” status are considered as important agricultural production areas. The main soil type in these areas is purple soil. This type of soil undergoes severe erosion and has a shallow layer and poor water retention capacity, which are the main factors limiting groundwater potential (Zhou et al., 2019). During the study period, the area under the “moderate” status initially increased and then decreased. From 2000–2010, the area under the “moderate” status showed an increase of  $53.24 \text{ km}^2$ , representing an increase rate of 0.89 %; this was mainly caused by mining and urban expansion. The area under the “moderate” status showed a decrease of  $183.17 \text{ km}^2$  from 2010–2020, representing a decrease rate of 3.05 %. This is likely due to the policies of returning farmlands to the forest (grass) areas and the agricultural structure adjustment implemented in the study area, which led to an increase in the vegetation coverage (Fig. 9d). Areas with high vegetation coverage can prolong the soil infiltration time and increase surface runoff, thereby effectively increasing the groundwater potential (Chen, 2014).

#### 5.1.4. “Good” status

Low-altitude areas are those under the “good” status; in these areas, the drainage density and vegetation coverage are relatively high. The area under the “good” status showed an increase of  $51.73 \text{ km}^2$  from 2000–2020, representing an increase rate of 1.24 %. This is likely due to the conversion of the areas under the “moderate” status to those under the “good” status owing to the large-scale implementation of the project aimed at converting farmlands to forest (grass) areas.

#### 5.1.5. “Very good” status

The areas under the “very good” status are distributed in the valleys of the Jinsha, Yalong, and Anning rivers. In these areas, the

drainage and fault density are large, and human activities are limited. These areas showed a decrease of 210.36 km<sup>2</sup> from 2000–2020, representing a decrease rate of 10.46 %; this was mainly caused by human activities.

### 5.2. Performance analysis of the evaluation model

The verification results prove that the new integrated method constructed using the CCM and PCA outperformed the CFMFs. Previous research demonstrates that an integrated model based on CT (including the CCM) is an objective method and can effectively deal with the nonlinear problem in evaluation indicators (Ghorbani et al., 2010; Zhan et al., 2013). PCA simplifies datasets by transforming multiple indicators into a few comprehensive indexes, and it can eliminate the mutual influence between indicators, which helps explain the spatial heterogeneity between indicators (Moshat et al., 2010; Kardanpour et al., 2014). Therefore, this study was conducted considering the natural and anthropogenic aspects, and a new groundwater potential evaluation method was constructed by combining the PCA and CCM. This new method mainly offers the following functions: 1) by utilizing the advantages of the CCM and PCA, the proposed evaluation method can fit complex nonlinear and discontinuity relationships between the groundwater potential and evaluation indicators and effectively solve the stratified spatial heterogeneity of the indicators and the uncertainty in the evaluation process; and 2) using the evaluation equation (Eq. 12), this method eliminates the weight restrictions on indicators, avoids human interference, and increases the objectivity of the results.

### 5.3. Limitations of the work

Although the obtained evaluation results are reliable and accurate, this study still involves a few limitations. The accuracy of the model depends not only on the learning algorithm but also on the parameters (Sun et al., 2020). However, the transition from  $m_{11}$  to  $m_{12}$  to 1 (Eq. 10) was set directly based on existing research, while neglecting the spatial characteristics of the transition amount (control variables are spatial data). Furthermore, evaluation indicators form the basis of groundwater potential evaluations; when certain indicators are not used, the evaluation results may be biased. For instance, this study used the spatial interpolation method to convert the precipitation data obtained from meteorological stations into raster data. This method is based on the assumption that the closer the spatial position, the more likely similar features. The known point data were used to estimate the unknown point data, which will affect the accuracy of results (Chen and Wang, 2020). Furthermore, the indicators that were difficult to quantify were neglected. For instance, the impact of implementing relevant policy management measures for the groundwater potential in mining areas was not considered.

However, despite these limitations, the evaluation results obtained in this study still provide useful information for the protection and sustainable management of groundwater resources in mining areas.

### 5.4. Wide applicability of the model

Groundwater potential depends on the combined action of several contributing factors, and the effect of these factors on the groundwater potential may vary from one region to another (Nasir et al., 2018). A previously proposed method for groundwater potential evaluation uses fixed weights for different locations of the study area, thus neglecting the spatial difference of the indicators' influences on the groundwater potential. This condition, to a certain extent, affects the accuracy of the evaluation results, especially when evaluating the groundwater potential at a regional scale. The primary feature of the model developed in this study is that it does not require the weight of the indicators and it considers the high flexibility and spatial difference of the indicators. Owing to this feature, the proposed model has wide applicability for groundwater potential evaluations.

Lastly, publicly available datasets were used in this study. To evaluate groundwater potential in other areas, appropriate indicators representing the type of human activity and the hydrogeological environment of the target area should be considered when developing the indicator system.

## 6. Conclusions

The accurate evaluation of the groundwater potential at the regional level is of great significance for the protection of groundwater resources, sustainable management, and land-use planning. Using the RS and GIS technologies, an evaluation indicator system considering natural and anthropogenic factors was established, in order to evaluate the groundwater potential in mining areas. Based on the CCM and PCA, a new model for the evaluation of the groundwater potential in mining areas was developed, and typical regions were selected for the evaluation and verification. The model developed in this study achieved satisfactory results and can be widely used in other areas with similar hydrological conditions. The evaluation results can also serve as data for local governments and related organizations to formulate water resource management plans and implement environmental governance and protection measures.

### Author statement

**Xiaofei Sun, Yingzhi Zhou and Xixi Lu:** Conceptualization, Methodology; **Linguo Yuan:** Data collection and processing; **Xiaofei Sun and Yingzhi Zhou:** Writing- Original draft preparation. **Huaiyong Shao:** Supervision; **Linguo Yuan:** Writing- Reviewing and Editing.

## Funding

This study was supported by the National Natural Science Foundation of China (Grant No.42074021), Department of Science and Technology of Sichuan Province (Grant Nos. 20ZDYF1142 and 2020JDTD0003), China Scholarship Council (CSC No.202007000081), and Science and Technology Bureau of Nanchong City (Grant Nos. 20YFZJ0029 and 19SXHZ0039).

## Declaration of Competing Interest

The authors report no declarations of interest.

## Acknowledgments

We thank the Sichuan Geological Survey Institute for providing the mining concession inventory and related data. My deepest thank also goes to Professor Batelaan (editor in chief of Journal of Hydrology: Regional Studies) and four anonymous reviewers for their insightful comments and suggestions.

## Appendix A. Supplementary data

Supplementary material related to this article can be found, in the online version, at doi:<https://doi.org/10.1016/j.ejrh.2021.100891>.

## References

- Aeschbach-Hertig, W., Gleeson, T., 2012. Regional strategies for the accelerating global problem of groundwater depletion. *Nat. Geosci.* 5, 853–861.
- Agarwal, R., Garg, P.K., 2016. Remote sensing and GIS based groundwater potential & recharge zones mapping using multi-criteria decision-making technique. *Water Resour. Manag.* 30, 243–260.
- Agarwal, E., Agarwal, R., Garg, R.D., Garg, P.K., 2013. Delineation of groundwater potential zone: an AHP/ANP approach. *J. Earth Syst. Sci.* 122, 887–898.
- Ahmed, K., Shahid, S., Harun, S., Ismail, T., Nawaz, N., Shamsudin, S., 2015. Assessment of groundwater potential zones in an arid region based on catastrophe theory. *Earth Sci. Inform.* 8 (3), 539–549.
- Al-Abadi, A.M., Shahid, S., 2015. A comparison between index of entropy and catastrophe theory methods for mapping groundwater potential in an arid region. *Environ. Monit. Assess.* 187, 576.
- Arulbalaji, P., Padmalal, D., Sreelash, K., 2019. GIS and AHP techniques based delineation of groundwater potential zones: a case study from southern Western Ghats. *India. Sci. Rep.* 9, 2082.
- Asar, Y., 2017. Some new methods to solve multicollinearity in logistic regression. *Commun. Stat. Simul. Comput.* 46, 2576–2586.
- Azimi, S., Azhdar Moghaddam, M., Hashemi Monfared, S.A., 2018. Spatial assessment of the potential of groundwater quality using fuzzy AHP in GIS. *Arab. J. Geosci.* 11, 142.
- Bargaoui, Z.K., Chebbi, A., 2009. Comparison of two kriging interpolation methods applied to spatiotemporal rainfall. *J. Hydrol.* 365, 56–73.
- Chen, B., 2014. Hydrological Response to Climate Change and LUCC Based on SWAT Model in Yanduhe Basin. Master's thesis. Central China Normal University.
- Chen, Y., Wang, J., 2020. Ecological security early-warning in central Yunnan Province, China, based on the gray model. *Ecol. Indic.* 111, 106000.
- Chen, W., Li, H., Hou, E., Wang, S., Wang, G., Panahi, M., Li, T., Peng, T., Guo, C., Niu, C., Xiao, L., Wang, J., Xie, X., Ahmad, B.B., 2018. GIS-based groundwater potential analysis using novel ensemble weights-of-evidence with logistic regression and functional tree models. *Sci. Total Environ.* 634, 853–867.
- Cheng, G., Wang, G.J., He, L., Lin, X.G., 2014. Parallelization for randomized forests used in human pose estimation. *Appl. Res. Comput.* 31, 1558–1561.
- Dai, J., 2016. Hydrogeological characteristics study and mine water inflow forecast of Taitian coal mine, Yanbian county of Panzhihua. *S. North Water Transfers Water Sci. Technol.* 14, 123–126.
- Dai, T.S., Sun, S.R., Zhao, W.H., Gu, B.Y., 2009. Evaluation of the sustainability of water resource system based on FAHP-PP model. *Resour. Environ. Yangtze Basin.* 18, 421–426.
- Ghorbani, M.A., Khatibi, R., Sivakumar, B., Cobb, L., 2010. Study of discontinuities in hydrological data using catastrophe theory. *Hydrol. Sci. J. J. Sci. Hydrol.* 55, 1137–1151.
- Gómez-Gutiérrez, Á., Conoscenti, C., Angileri, S.E., Rotigliano, E., Schnabel, S., 2015. Using topographical attributes to evaluate gully erosion proneness (susceptibility) in two Mediterranean basins: advantages and limitations. *Nat. Hazards Dordr. (Dordr.)* 79, 291–316.
- Grigg, A.H., 2017. Hydrological response to bauxite mining and rehabilitation in the jarrah forest in south west Australia. *J. Hydrol. Reg. Stud.* 12, 150–164.
- Gyeltschen, S., Tran, T.V., Teja Gunda, G.K., Kannaujiya, S., Chatterjee, R.S., Champatiray, P.K., 2020. Groundwater potential zones using a combination of geospatial technology and geophysical approach: case study in Dehradun, India. *Hydrol. Sci. J.* 65, 169–182.
- Huan-cheng, M.A., McConchie, J.A., 2001. The dry-hot valleys and forestation in southwest China. *J. For. Res.* 12, 35–39.
- Jenifer, M.A., Jha, M.K., 2017. Comparison of analytic hierarchy process, catastrophe and entropy techniques for evaluating groundwater prospect of hard-rock aquifer systems. *J. Hydrol. (Amst)* 548, 605–624.
- Jha, M.K., 2013. Sustainable management of groundwater resources in developing countries: constraints and challenges. *on a Sustainable Future of the Earth's Natural Resources*. Springer, Berlin, Heidelberg, pp. 325–348.
- Jiang, J.F., 2005. The application of GIS-based regional groundwater resource evaluation mode. *J. Shenyang Agric. Univ.* 36, 367–369.
- Kardanpour, Z., Jacobsen, O.S., Esbensen, K.H., 2014. Soil heterogeneity characterization using PCA (Xvariogram)-multivariate analysis of spatial signatures for optimal sampling purposes. *Chemometr. Intell. Lab. Syst.* 136, 24–35.
- Karimi, V., Khatibi, R., Ghorbani, M.A., Bui, D.T., Darbandi, S., 2020. Strategies for learning groundwater potential modelling indices under sparse data with supervised and unsupervised techniques. *Water Resour. Manag.* 34, 2389–2417.
- Kordestani, M.D., Naghibi, S.A., Hashemi, H., Ahmadi, K., Kalantar, B., Pradhan, B., 2019. Groundwater potential mapping using a novel data-mining ensemble model. *Hydrogeol. J.* 27, 211–224.
- Krishnamurthy, J., Mani, A., Jayaraman, V., Manivel, M., 2000. Groundwater resources development in hard rock terrain - an approach using remote sensing and GIS techniques. *Int. J. Appl. Earth Obs. Geoinf.* 2, 204–215.
- Krizhevsky, A., Sutskever, I., Hinton, G.E., 2012. Imagenet classification with deep convolutional neural networks, in: *adv. Neural Inf. Process. Syst.* 1097–1105.

- Kumar, A., Krishna, A.P., 2018. Assessment of groundwater potential zones in coal mining impacted hard-rock terrain of India by integrating geospatial and analytic hierarchy process (AHP) approach. *Geocarto Int.* 33, 105–129.
- Kumar, T., Gautam, A.K., Kumar, T., 2014. Appraising the accuracy of GIS-based multi-criteria decision-making technique for delineation of groundwater potential zones. *Water Resour. Manag.* 28, 4449–4466.
- Lee, S., Lee, K.K., Yoon, H., 2019. Using artificial neural network models for groundwater level forecasting and assessment of the relative impacts of influencing factors. *Hydrogeol. J.* 27, 567–579.
- Lerner, D.N., Harris, B., 2009. The relationship between land use and groundwater resources and quality. *Land Use Policy* 26, S265–S273.
- Liu, J., Bao, J., Yin, Y., Yang, S., 2015. Applications of catastrophe theory in engineering: a review. *J. Comput. Theor. Nanosci.* 12, 5739–5744.
- Liu, Y., Huang, C., Wang, Q., Luan, J., Ding, M., 2018. Assessment of sustainable livelihood and geographic detection of settlement sites in ethnically contiguous poverty-stricken areas in the Aba Prefecture, China. *ISPRS Int. J. Geo Inf.* 7, 16.
- Manap, M.A., Nampak, H., Pradhan, B., Lee, S., Sulaiman, W.N.A., Ramli, M.F., 2014. Application of probabilistic-based frequency ratio model in groundwater potential mapping using remote sensing data and GIS. *Arab. J. Geosci.* 7, 711–724.
- Moghaddam, D.D., Rahmati, O., Panahi, M., Tiefenbacher, J., Darabi, H., Haghizadeh, A., Haghghi, A.T., Nalivan, O.A., Tien Buiq, D.T., 2020. The effect of sample size on different machine learning models for groundwater potential mapping in mountain bedrock aquifers. *CATENA* 187, 104421.
- Moshat, S., Datta, S., Bandyopadhyay, A., Pal, P., 2010. Optimization of CNC end milling process parameters using PCA-based Taguchi method. *Int. Res. J. Eng. Sci. Technol. Innov.* 2, 95–102.
- Murmu, P., Kumar, M., Lal, D., Sonker, I., Singh, S.K., 2019. Delineation of groundwater potential zones using geospatial techniques and analytical hierarchy process in Dumka district, Jharkhand, India. *Groundwater Sustain. Dev.* 9, 100239.
- Naghibi, S.A., Ahmadi, K., Daneshi, A., 2017a. Application of support vector machine, random forest, and genetic algorithm optimized random forest models in groundwater potential mapping. *Water Resour. Manag.* 31, 2761–2775.
- Naghibi, S.A., Moghaddam, D.D., Kalantar, B., Pradhan, B., Kisi, O., 2017b. A comparative assessment of GIS-based data mining models and a novel ensemble model in groundwater well potential mapping. *J. Hydrol.* 548, 471–483.
- Naghibi, S.A., Dolatkordestani, M., Rezaei, A., Amouzegari, P., Heravi, M.T., Kalantar, B., Pradhan, B., 2019. Application of rotation forest with decision trees as base classifier and a novel ensemble model in spatial modeling of groundwater potential. *Environ. Monit. Assess.* 191, 248.
- Nasir, M.J., Khan, S., Zahid, H., Khan, A., 2018. Delineation of groundwater potential zones using GIS and multi influence factor (MIF) techniques: a study of district Swat, Khyber Pakhtunkhwa, Pakistan. *Environ. Earth Sci.* 77, 1–11.
- Nguyen, P.T., Ha, D.H., Jaafar, A., Nguyen, H.D., Van Phong, T., Al-Ansari, N., Prakash, I., Le, H.V., Pham, B.T., 2020. Groundwater potential mapping combining artificial neural network and real AdaBoost ensemble technique: the DakNong Province case-study, Vietnam. *Int. J. Environ. Res. Public Health.* 17, 2473.
- Oh, H.J., Kim, Y.S., Choi, J.K., Park, E., Lee, S., 2011. GIS mapping of regional probabilistic groundwater potential in the area of Pohang City, Korea. *J. Hydrol.* 399, 158–172.
- Okadera, T., Wang, Q.X., Deni, E., Nakayama, T., 2019. Groundwater monitoring for evaluating the pasture carrying capacity and its vulnerability in arid and semi-arid regions: a case study of urban and mining areas in Mongolia. In: IOP Conference Series. Earth and Environmental Science (Vol. 266, No. 1, p. 012013). IOP Publishing.
- Ozdemir, A., 2011. Using a binary logistic regression method and GIS for evaluating and mapping the groundwater spring potential in the Sultan Mountains (Aksehir, Turkey). *J. Hydrol.* 405, 123–136.
- Pigato, M., Tang, W., 2015. China and Africa.
- Poon, B., Ashraful Amin, M.A., Yan, H., 2011. Performance evaluation and comparison of PCA based human face recognition methods for distorted images. *Int. J. Mach. Learn. & Cyber.* 2, 245–259.
- Post, D.A., Crosbie, R.S., Viney, N.R., Peeters, L.J.M., Zhang, Y.Q., Herron, N.F., Wilkins, A., Janardhanan, S., Karim, F., Aryal, S.K., Pena-Arcibia, J., Lewis, S., Evans, T., Vaze, J., Chiew, F.H.S., Marvanek, S.P., Henderson, B., Schmidt, B., Herr, A., 2020. Impacts of coal mining and coal seam gas extraction on groundwater and surface water. *J. Hydrol.* 591, 125281.
- Pradhan, B., 2013. A comparative study on the predictive ability of the decision tree, support vector machine and neuro-fuzzy models in landslide susceptibility mapping using GIS. *Comput. Geosci.* 51, 350–365.
- Punmia, B., Jain, A.K., 2005. Soil Mechanics and Foundations. Firewall Media.
- Razandi, Y., Pourghasemi, H.R., Neisani, N.S., Rahmati, O., 2015. Application of analytical hierarchy process, frequency ratio, and certainty factor models for groundwater potential mapping using GIS. *Earth Sci. Inform.* 8, 867–883.
- Rizeei, H.M., Pradhan, B., Saharkhiz, M.A., Lee, S., 2019. Groundwater aquifer potential modeling using an ensemble multi-adoptive boosting logistic regression technique. *J. Hydrol.* 579, 124172.
- Sadeghfam, S., Hassanzadeh, Y., Nadiri, A.A., Khatibi, R., 2016. Mapping groundwater potential field using catastrophe fuzzy membership functions and Jenks optimization method: a case study of Maragheh-bonab Plain, Iran. *Environ. Earth Sci.* 75, 545.
- Sadeghfam, S., Khatibi, R., Dadashi, S., Nadiri, A.A., 2020a. Transforming subsidence vulnerability indexing based on ALPRIFT into risk indexing using a new fuzzy-catastrophe scheme. *Environ. Impact Assess. Rev.* 82, 106352.
- Sadeghfam, S., Khatibi, R., Daneshfaraz, R., Borhan Rashidi, H.B., 2020b. Transforming vulnerability indexing for saltwater intrusion into risk indexing through a fuzzy catastrophe scheme. *Water Resour. Manag.* 34, 175–194.
- Sadeghfam, S., Khatibi, R., Nadiri, A.A., Ghodsi, K., 2021. Next stages in aquifer vulnerability studies by integrating risk indexing with understanding uncertainties by using generalised likelihood uncertainty estimation. *Expo. Health.* 1–15.
- Sahoo, S., Dhar, A., Kar, A., Ram, P., 2017. Grey analytic hierarchy process applied to effectiveness evaluation for groundwater potential zone delineation. *Geocarto Int.* 32, 1188–1205.
- Serele, C., Pérez-Hoyos, A., Kayitakire, F., 2020. Mapping of groundwater potential zones in the drought-prone areas of south Madagascar using geospatial techniques. *Geosci. Front.* 11, 1403–1413.
- Shao, H., Liu, M., Shao, Q., Sun, X., Wu, J., Xiang, Z., Yang, W., 2014. Research on eco-environmental vulnerability evaluation of the Anning River Basin in the upper reaches of the Yangtze River. *Environ. Earth Sci.* 72, 1555–1568.
- Shao, H., Sun, X., Lin, Y., Xian, W., Zhou, Y., Yuan, L., Qi, J., 2021. A method for spatio-temporal process assessment of eco-geological environmental security in mining areas using catastrophe theory and projection pursuit model. *Prog. Phys. Geogr.* 0309133320982542.
- Singh, R.K., Murty, H.R., Gupta, S.K., Dikshit, A.K., 2009. An overview of sustainability assessment methodologies. *Ecol. Indic.* 9, 189–212.
- Sun, D., Wen, H., Wang, D., Xu, J., 2020. A random forest model of landslide susceptibility mapping based on hyperparameter optimization using Bayes algorithm. *Geomorphology* 362, 107201.
- Thapa, R., Gupta, S., Guin, S., Kaur, H., 2017. Assessment of groundwater potential zones using multi-influencing factor (MIF) and GIS: a case study from Birbhum district, West Bengal. *Appl. Water Sci.* 7, 4117–4131.
- Todd, D.K., Mays, L.W., 2005. *Groundwater Hydrology*, third ed. John Wiley & Sons, New Jersey, p. 636.
- Tsegaye, T., Sheppard, D., Islam, K.R., Tadesse, W., Atalay, A., Marzen, L., 2006. Development of chemical index as a measure of in-stream water quality in response to land-use and land cover changes. *Water Air Soil Pollut.* 174, 161–179. <https://doi.org/10.1007/s11270-006-9090-5>.
- Wang, D., Wang, F., Huang, Y., Duan, X., Liu, J., Hu, B., Sun, Z., Chen, J., 2018. Examining the effects of hydropower station construction on the surface temperature of the Jinsha River Dry-Hot Valley at different seasons. *Remote Sens.* 10, 600.
- Wen, B.J., Chen, Y.C., Wang, G.S., Dai, T., 2019. China's demand for energy and mineral resources by 2035. *Strategic Study Chinese Acad. Eng.* 21, 68–73.
- Wu, S.K., Zhang, Y.H., 2019. Distribution and management policy of energy resource bases in China. *Strategic Study Chinese Acad. Eng.* 21, 81–87.
- Yeh, H.F., Lee, C.H., Hsu, K.C., Chang, P.H., 2009. GIS for the assessment of the groundwater recharge potential zone. *Environ. Geol.* 58, 185–195.
- Yesilnacar, E., Topal, T., 2005. Landslide susceptibility mapping: a comparison of logistic regression and neural networks methods in a medium scale study, Hendek region (Turkey). *Eng. Geol.* 79, 251–266.

- Yilmaz, I., 2009. Landslide susceptibility mapping using frequency ratio, logistic regression, artificial neural networks and their comparison: a case study from Kat landslides (Tokat—turkey). *Comput. Geosci.* 35, 1125–1138.
- Zeeman, E.C., 1979. Catastrophe theory. Springer Series in Synergetics. Springer, Berlin, Heidelberg, pp. 12–22.
- Zhan, W., Shang, Y.Q., Chi, F.X., 2013. Application of Catastrophe Theory in Traffic Flow of Highway Tunnel Group. Trans Tech Publications Ltd. AMR, pp. 734–737.
- Zheng, J.X., 2012. Study on sustainable development of mineral resources of China. *China Min. Mag.* 1, 34–36.
- Zhong, X.H., 2000. Degradation of ecosystem and ways of its rehabilitation and reconstruction in dry and hot valley—take representative area of Jinsha river, Yunnan Province as an example. *Resour. Environ. Yangtze Basin.* 9, 376–383.
- Zhou, Q., Wang, L.C., Xing, L., Ma, S.M., Zhang, X.D., Chen, J., Shi, C., 2019. Effects of Chinese milk vetch intercropped with rape under straw mulching on soil aggregate and organic carbon character. *Chin. J. Appl. Ecol.* 30, 1235–1242.
- Zhu, Z.K., 2014. Floor Water Inrush Prediction Based on Risk Evaluation and Catastrophe Theory. Doctoral dissertation. China University of Mining and Technology.
- Zhu, C.C., Han, Y.J., Liu, P.G., Zhu, J., 2014. Analysis on influence of interfering exploitation in the adjacent mine mountains on groundwater. *Undergr. Water.* 4, 99–102.
- Zhu, G., Wu, X., Ge, J., Liu, F., Zhao, W., Wu, C., 2020. Influence of mining activities on groundwater hydrochemistry and heavy metal migration using a self-organizing map (SOM). *J. Cleaner Prod.* 257, 120664.
- Zipkin, E.F., Grant, E.H.C., Fagan, W.F., 2012. Evaluating the predictive abilities of community occupancy models using AUC while accounting for imperfect detection. *Ecol. Appl.* 22, 1962–1972.